An isogeometric collocation approach for Bernoulli-Euler beams and Kirchhoff plates

Alessandro Reali[a], Hector Gomez[b,*]

[a] *Department of Civil Engineering and Architecture, University of Pavia, via Ferrata 3, 27100, Pavia, Italy*
[b] *Departamento de Métodos Matemáticos, Universidade da Coruña, Campus de A Coruña, 15071, A Coruña, Spain*

Abstract

In this paper, IGA collocation methods are for the first time introduced for the solution of thin structural problems described by Bernoulli-Euler beam and Kirchhoff plate models. In particular, a precise description of the proposed methods, of the relevant implementation details, and of the strategy to efficiently deal with different combinations of boundary conditions is given. Finally, several numerical experiments confirm that the proposed formulations represent an efficient and geometrically flexible tool for the simulation of thin structures.

Keywords: Collocation, Bernoulli-Euler beam, Kirchhoff plate, NURBS, Isogeometric analysis

1. Introduction

Isogeometric analysis (IGA) is a recently proposed computational technology, introduced by Hughes *et al.* [14, 29] in 2005, with the main aim of bridging the gap between Computer Aided Design (CAD) and Finite Element Analysis (FEA). The basic IGA paradigm consists of adopting the same basis functions used for geometry representations in CAD systems - such as, e.g., Non-Uniform Rational B-Splines (NURBS) - for the approximation of field variables, in an isoparametric fashion. This leads to a cost-saving simplification of the typically expensive mesh generation and refinement processes required by standard FEA, which was the original motivation for IGA. Moreover, thanks to the high-regularity properties of its basis functions, IGA has shown a better accuracy per-degree-of-freedom and an enhanced robustness with respect to standard FEA in a number of applications ranging from solids and structures [5, 11, 13, 15, 16, 17, 18, 21, 30, 31, 37, 38, 39] to fluids [1, 8, 9, 12, 19, 23, 24], opening also the door to geometrically flexible discretizations of higher-order partial differential equations in primal form (see, e.g., [2, 22, 25, 26, 27, 35, 36]).

An important issue when dealing with IGA regards the development of efficient integration rules, able to reduce assembly costs in particular when higher-order approximations are employed. The fact that element-wise Gauss quadrature, typically used for standard FEA and originally adopted for Galerkin-based IGA, does not properly take into account the inter-element higher continuity of the IGA basis functions leads to sub-optimal assembly costs, which significantly affect the performance of IGA methods. *Ad-hoc* quadrature rules have been proposed in [7, 32, 41], but the development of a general and effective solution for Galerkin-based IGA methods is still an open problem.

Aiming at optimizing the computational cost, still taking advantage of IGA geometrical flexibility and accuracy, isogeometric collocation schemes have been recently proposed in [3, 4]. The basic idea consists of

Corresponding author. Email: hgomez@udc.es

the discretization of the governing partial differential equations in strong form, adopting the isoparametric paradigm and making use of the higher-continuity properties of the IGA shape functions. Detailed comparisons with both IGA and FEA Galerkin-based approaches have shown IGA collocation advantages in terms of accuracy versus computational cost, in particular when higher-order approximation degrees are adopted [40]. In general, IGA collocation features look particularly desirable in all those situations where evaluation and assembly costs are dominant. This is the case of explicit structural dynamics where the computational cost is dominated by stress divergence evaluations at quadrature points for the calculation of the residual force vector [4].

Within the IGA collocation context, several promising significant studies have been recently published, including phase-field modeling [28], contact [20], and hierarchical local refinement [40]. In particular, IGA collocation offers interesting possibilities in the framework of shear-deformable structural elements. Three-field (i.e., displacements, rotations, shear stresses) mixed formulations for Timoshenko initially-straight planar beams [10] and for curved spatial rods [6] have been successfully proposed. In such cases, the structure of IGA collocation leads to mixed methods which are locking-free independently of the approximation degrees for the three fields. Such a unique property has been proven analytically and extensively tested numerically. Following these positive results, isogeometric collocation has been then successfully applied also to the solution of Reissner-Mindlin plate problems, in both primal and mixed forms [33]. Finally, an interesting new single-parameter formulation for shear-deformable beams, recently introduced in [34], has been solved also via IGA collocation.

In the present paper, we introduce IGA collocation methods for the solution of thin structural problems described by Bernoulli-Euler beam and Kirchhoff plate models. Such models are described by fourth-order differential equations, for which IGA collocation has already been shown to be an efficient and viable solution scheme in the context of Cahn-Hilliard phase-field modeling. With respect to [28], an enhanced strategy to efficiently deal with all relevant combinations of boundary conditions typical of plate problems is herein introduced. Several numerical experiments confirm the good behavior of the proposed formulations.

The paper is organized as follows. In the second section, the simple model problem of a Bernoulli-Euler beam is considered. After the introduction of the boundary-value problem, the proposed numerical formulation based on IGA collocation is presented and numerically tested. In the third section, Kirchhoff plates are considered. The boundary-value problem is stated and the adopted numerical formulation is discussed in detail, with special attention to the strategy for boundary condition imposition. The fourth section is then devoted to numerical tests showing the performance of the proposed collocation method for Kirchhoff plates, while, in the last section, conclusions are drawn.

2. Bernoulli-Euler beams

We start illustrating the simple one-dimensional case represented by an initially straight Bernoulli-Euler beam problem. The differential equation governing the boundary-value problem is of fourth order and we solve it in strong form by means of an isogeometric collocation scheme. As we will point out later, the

theoretical analysis provided in [3] for second-order problems can be easily extended to this case, guaranteeing the convergence of the method. In this section, we introduce the boundary-value problem in strong form, we describe the proposed numerical formulation based on isogeometric collocation, and we present numerical examples showing the good behavior of the method.

2.1. Boundary-value problem

The boundary-value problem associated with a Bernoulli-Euler beam can be stated as follows. Let $L > 0$ be the length of the beam and let us assume that $\Omega = (0, L)$ is the problem domain. The boundary of Ω is denoted by $\Gamma = \{0\} \cup \{L\}$. We assume that Γ admits decompositions $\Gamma = \overline{\Gamma_w \cup \Gamma_Q}$ and $\Gamma = \overline{\Gamma_\varphi \cup \Gamma_M}$ with $\Gamma_w \cap \Gamma_Q = \emptyset$, $\Gamma_\varphi \cap \Gamma_M = \emptyset$, where $\emptyset$ denotes the empty set. To ensure the well-posedness of the problem, we impose the constraint $\Gamma_w \neq \emptyset$, but we note that Γ_Q, Γ_φ and Γ_M are allowed to be the empty set. Then, the problem can be stated as: given $f : \Omega \mapsto \mathbb{R}$, $w_\Gamma : \Gamma_w \mapsto \mathbb{R}$, $\varphi_\Gamma : \Gamma_\varphi \mapsto \mathbb{R}$, $Q_\Gamma : \Gamma_Q \mapsto \mathbb{R}$, and $M_\Gamma : \Gamma_M \mapsto \mathbb{R}$, find $w : \Omega \mapsto \mathbb{R}$ such that,

$$EI\frac{\mathrm{d}^4 w}{\mathrm{d}x^4} = f \qquad \text{in} \quad \Omega \tag{1}$$

$$w = w_\Gamma \qquad \text{on} \quad \Gamma_w \tag{2}$$

$$-\frac{\mathrm{d}w}{\mathrm{d}x} = \varphi_\Gamma \qquad \text{on} \quad \Gamma_\varphi \tag{3}$$

$$EI\frac{\mathrm{d}^3 w}{\mathrm{d}x^3} = Q_\Gamma \qquad \text{on} \quad \Gamma_Q \tag{4}$$

$$EI\frac{\mathrm{d}^2 w}{\mathrm{d}x^2} = M_\Gamma \qquad \text{on} \quad \Gamma_M \tag{5}$$

Here, $E > 0$ is the Young's modulus and $I > 0$ is the beam's moment of inertia, and we have assumed that the product EI is constant. The function f denotes a load per unit length, w is the deflection of the beam, and x denotes the spatial coordinate. Adopting standard structural-mechanics notations, we can obtain the cross section rotation as $\varphi = -\dfrac{\mathrm{d}w}{\mathrm{d}x}$, the shear force as $Q = EI\dfrac{\mathrm{d}^3 w}{\mathrm{d}x^3}$, and the bending moment as $M = EI\dfrac{\mathrm{d}^2 w}{\mathrm{d}x^2}$. Accordingly, boundary conditions (2)–(5) may be interpreted as imposed deflection, rotation, shear force, and bending moment, respectively. Note that not all of them apply simultaneously.

Remark:

The boundary-value problem (1)–(5) encompasses a number of cases of engineering interest. For example, a beam clamped at $x = 0$ and simply supported at $x = L$ would be defined by $\Gamma_w = \Gamma = \{0\} \cup \{L\}$, $\Gamma_\varphi = \{0\}$, $\Gamma_M = \{L\}$, and $w_\Gamma = \varphi_\Gamma = M_\Gamma = 0$. Note that these conditions automatically define Γ_Q as the empty set.

2.2. Numerical formulation

Our numerical formulation is based on isogeometric collocation. In the context of beams, our collocation method can be derived from one-dimensional B-Splines, which we define in the next Section.

2.2.1. One-dimensional B-Splines

One-dimensional B-Splines are piece-wise polynomials. They can be defined as linear combinations of a B-Spline basis. Let us assume that we work on a parametric space $\xi \in \mathcal{I}$, where $\mathcal{I}$ is a closed interval of $\mathbb{R}$. To define a B-Spline basis, the degree of the engendering polynomial p and the so-called *knot vector* $\boldsymbol{\Xi}$ need to be specified. The entries of the knot vector $\boldsymbol{\Xi}$, which are called knots, are non-decreasing coordinates of the parametric space, so that

$$\boldsymbol{\Xi} = (\xi_1, \xi_2, \ldots, \xi_{n+p+1}). \tag{6}$$

Throughout this paper, we will assume the knot vector to be *open*, that is, $\xi_1 = \ldots = \xi_{p+1}$ and $\xi_{n+1} = \ldots = \xi_{n+p+1}$. The zeroth degree B-Spline functions $\{N_{i,0}\}_{i=1,\ldots,n}$ are defined as

$$N_{i,0}(\xi) = \begin{cases} 1 & \text{if} \quad \xi_i \leq \xi < \xi_{i+1} \\ 0 & \text{otherwise} \end{cases} \quad ; \quad i = 1, \ldots, n. \tag{7}$$

The p-th degree B-Spline basis functions are defined recursively using the relation

$$N_{i,q}(\xi) = \frac{\xi - \xi_i}{\xi_{i+p} - \xi_i} N_{i,q-1}(\xi) + \frac{\xi_{i+p+1} - \xi}{\xi_{i+p+1} - \xi_{i+1}} N_{i+1,q-1}(\xi); \quad i = 1, \ldots, n; \quad q = 1, \ldots, p. \tag{8}$$

The functions $\{N_{i,p}\}_{i=1,\ldots,n}$ are $\mathcal{C}^\infty$ everywhere except at the knots. At a non-repeated knot, the functions have $p-1$ continuous derivatives. If a knot has multiplicity k, the number of continuous derivatives at that point is $p-k$.

B-Spline functions in the parameter space can be pushed forward onto a physical space using a geometrical mapping. However, for the sake of simplicity, in the case of Bernoulli-Euler beams, we will work on the parameter space, as the role of geometrical mapping is not so important in this case. The possibility of using mapped geometries in our algorithm will be obvious when we deal with Kirchhoff plates. Thus, for Bernoulli-Euler beams, our discrete space is simply

$$\mathcal{S}^h = \text{span}\{N_{i,p}(\xi), i = 1, \ldots, n\} \tag{9}$$

where the superscript h refers to a length scale which is representative of the level of refinement of the discretization. We note that $\dim(\mathcal{S}^h) = n$. Functions of $\mathcal{S}^h$ can be constructed by linear combinations of the basis functions. Thus, $w \in \mathcal{S}^h$ can be written as $w(\xi) = \sum_{A=1}^{n} w_A N_{A,p}(\xi)$, where the w_A's are called *control variables* in the isogeometric-analysis parlance. Note also that the function w is interpolatory at the domain boundaries, that is, $w(\xi_1) = w_1$, and $w(\xi_{n+p+1}) = w_n$.

2.2.2. Collocation strategy

To simplify the notation, let us suppose, without loss of generality, that $\xi_1 = 0$ and $\xi_{n+p+1} = L$, so that $\xi = x$, and the parameter space and the physical space are one and the same. We will also assume $p \geq 4$. In our algorithm, displacement boundary conditions are strongly enforced in the discrete space. Thus, let us define the space $\mathcal{S}_d^h = \{w^h \in \mathcal{S}^h | w^h = w_\Gamma \text{ on } \Gamma_w\}$. Since the basis $\{N_{i,p}\}_{i=1,\ldots,n}$ is interpolatory at the boundary, a function of $\mathcal{S}_d^h$ can be constructed by taking a function of $\mathcal{S}^h$ and constraining the control variable(s) w_1 and/or w_n to take the value of w_Γ at $x = 0$ and/or $x = L$. For example, if $\Gamma_w = \{0\}$, a function of $\mathcal{S}_d^h$ can be constructed as $w^h(\xi) = w_\Gamma(0) N_{1,p}(\xi) + \sum_{A=2}^{n} w_A N_{A,p}(\xi)$.

Let us call n_d the number of displacement boundary conditions in the boundary-value problem (1)–(5). Thus, if $\Gamma_w = \{0\}$ or $\Gamma_w = \{L\}$, then $n_d = 1$. If $\Gamma_w = \{0\} \cup \{L\}$, then $n_d = 2$. Note that $\dim(\mathcal{S}_d^h) = n - n_d$. Once the displacement boundary conditions have been strongly enforced into the discrete space, we need $n - n_d$ independent equations to determine the remaining control variables. To obtain a well-posed boundary-value problem for a fourth-order differential equation, we need to impose 2 boundary conditions at each point of the boundary. Therefore, once the displacement boundary conditions have been enforced in the space, we have $4 - n_d$ remaining equations for boundary conditions. In our algorithm, these equations are obtained by collocating the remaining boundary equations at the boundary points where they hold. Thus, after all boundary conditions have been imposed, we have $\dim(\mathcal{S}_d^h) - (4 - n_d) = n - 4$ remaining equations to enforce Eq. (1). To this end, we define the Greville abscissae associated to the knot vector $\boldsymbol{\Xi} = (\xi_1, \xi_2, \ldots, \xi_{n+p+1})$, as follows

$$\hat{\tau}_i = \frac{1}{p} \sum_{j=1}^{p} \xi_{i+j};\ i = 1, \ldots, n \tag{10}$$

Note that there are n Greville points associated to the knot vector $\boldsymbol{\Xi}$. Note also that, for an open knot vector, the first and the last Greville points lie on the boundary, that is, $\hat{\tau}_1 = \xi_1 = 0$ and $\hat{\tau}_n = \xi_{n+p+1} = L$. In our collocation strategy, $\hat{\tau}_1$ and $\hat{\tau}_n$ have been used at least once to collocate some of the boundary conditions (3)–(5). The Greville points $\hat{\tau}_2$ and $\hat{\tau}_{n-1}$ are *disregarded* in our collocation scheme. The remaining $n - 4$ collocation points, that is, $\{\hat{\tau}_3, \ldots, \hat{\tau}_{n-2}\}$ are used to impose Eq. (1). This completely defines our collocation algorithm for Bernoulli-Euler beams.

Remark:

Let us assume that the beam is clamped at $x = 0$ and simply supported at $x = L$, which corresponds to the case $\Gamma_w = \Gamma = \{0\} \cup \{L\}$, $\Gamma_\varphi = \{0\}$, $\Gamma_M = \{L\}$, and $w_\Gamma = \varphi_\Gamma = M_\Gamma = 0$. In this particular case, our collocation scheme would make use of the discrete space $\mathcal{S}_d^h = \text{span}\{N_{i,p}(\xi), i = 2, \ldots, n-1\}$, and, thus, $w^h = \sum_{A=2}^{n-1} w_A N_{A,p}(\xi)$. The discrete problem is stated as: find $\{w_A\}_{A=2,\ldots,n-1}$ such that

$$EI \frac{\mathrm{d}^4 w^h}{\mathrm{d}x^4}(\hat{\tau}_i) = f(\hat{\tau}_i),\ i = 3, \ldots, n-2 \tag{11}$$

$$-\frac{\mathrm{d}w^h}{\mathrm{d}x}(\hat{\tau}_1) = 0 \tag{12}$$

$$EI \frac{\mathrm{d}^2 w^h}{\mathrm{d}x^2}(\hat{\tau}_n) = 0 \tag{13}$$

Eqs. (11)–(13) define a square linear system of equations.

2.2.3. Theoretical results

In the first paper appeared on isogeometric collocation [3], the authors analytically proved optimal convergence (i.e., of order $p - 1$) of isogeometric collocations schemes in the $W^{2,\infty}$-norm in the context of 1D second-order differential problems. In addition, in the same paper, it was numerically observed that orders of convergence p or $p - 1$ were attained in both $W^{1,\infty}$- and L^∞-norms (or, equivalently, in H^1- and L^2-norms) for even or odd degree p, respectively. All these results have been numerically proven to hold also in higher dimensions.

Recasting the same arguments in the context of 1D fourth-order differential problems, the aforementioned proof can be straightforwardly extended to the case under consideration in this paper, guaranteeing optimal convergence (i.e., of order $p-3$) in the $W^{4,\infty}$-norm. Such a result has been successfully numerically validated.

Moreover, analogously to what was observed in the context of second-order problems, it is natural to expect that orders of convergence $p-2$ or $p-3$ are attained, for even or odd degree p, respectively, for all engineering relevant quantities (i.e., deflections, rotations, bending moments, and shear forces) in, e.g., L^2-norm. Such a conjecture is numerically confirmed in the following section.

2.3. Numerical examples

The convergence behavior of the proposed formulation is numerically tested on a simple model problem consisting of a simply supported beam with a distributed sinusoidal load, for which the analytical solution can be easily computed.

The boundary-value problem under consideration reads as

$$EI\frac{\mathrm{d}^4 w}{\mathrm{d}x^4} = 16\pi^4 \sin(2\pi x) \quad \text{in} \quad \Omega \tag{14}$$

$$w = 0 \quad \text{on} \quad \Gamma_w \tag{15}$$

$$EI\frac{\mathrm{d}^2 w}{\mathrm{d}x^2} = 0 \quad \text{on} \quad \Gamma_M \tag{16}$$

with $EI = 1$, $L = 1$, $\Gamma_w = \Gamma = \{0\} \cup \{L\}$, and $\Gamma_M = \Gamma = \{0\} \cup \{L\}$. The analytical solution for the quantities of engineering interest is $w = \sin(2\pi x)$, $\varphi = -2\pi\cos(2\pi x)$, $Q = -8\pi^3 EI\cos(2\pi x)$, and $M = -4\pi^2 EI\sin(2\pi x)$. Convergence plots of the L^2-norm error for w, φ, Q, and M are reported in Figure 1 for degrees $p = 4, \dots, 9$. It is possible to observe that the expected orders of convergence (i.e., $p-2$ or $p-3$ for even or odd degree p, respectively) are attained, and that for all quantities a very similar convergence behavior is in general obtained.

Moreover, we performed several further numerical experiments to check the convergence behavior of the formulation with different combinations of boundary conditions. In all tests, the convergence rates highlighted above were attained (the results are not reported here for the sake of brevity).

3. Kirchhoff plates

We now focus on the more complex problem of Kirchhoff plates, consisting of a 2D fourth-order boundary-value problem governed by the bi-Laplace (or biharmonic) operator.

As anticipated in the introduction, the numerical approximation of fourth-order partial differential equations by means of isogeometric collocation was already proposed by the authors of this paper in the context of Cahn-Hilliard phase field modeling [28]. It is however worth to devote a special attention to the specific problem of Kirchhoff plates, given its significance in engineering applications. In particular, a delicate point in this framework is the capability of correctly imposing the different boundary conditions that may arise in

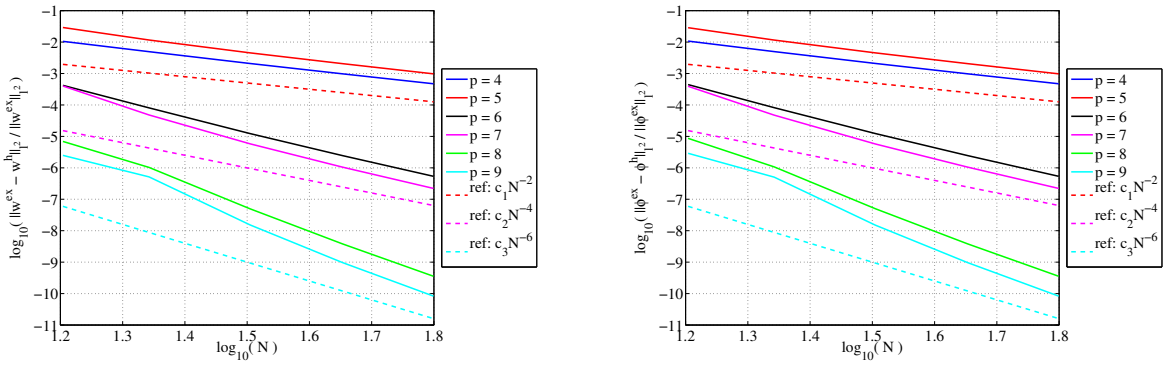

(a) Deflection

(b) Rotation

(c) Shear force

(d) Bending moment

Figure 1: (Color online) Simply supported beam with a distributed sinusoidal load. Convergence plots of the L^2-norm error for w (a), φ (b), Q (c), and M (d) as a function of the number of control points N and for different degrees p.

plate problems, where the technique proposed in [28] may not be sufficiently flexible. Therefore, in the following, we also propose an enhanced technique to efficiently deal with all relevant combinations of boundary conditions.

We finally carefully validate the proposed formulation by means of several significant numerical experiments, presented in the next section.

3.1. Boundary-value problem

The boundary-value problem associated with a Kirchhoff plate can be stated as follows. Let Ω be an open subset of $\mathbb{R}^2$. We assume that Ω has a sufficiently smooth boundary Γ with a well-defined normal $\boldsymbol{n}$. Analogously to the one-dimensional case, we assume that Γ can be decomposed as $\Gamma = \overline{\Gamma_w \cup \Gamma_Q}$ and $\Gamma = \overline{\Gamma_\varphi \cup \Gamma_M}$ with $\Gamma_w \neq \emptyset$; $\Gamma_w \cap \Gamma_Q = \emptyset$, $\Gamma_\varphi \cap \Gamma_M = \emptyset$. We state the following boundary-value problem over the spatial domain Ω: given the functions $g : \Omega \mapsto \mathbb{R}$, $w_\Gamma : \Gamma_w \mapsto \mathbb{R}$, $\varphi_\Gamma : \Gamma_\varphi \mapsto \mathbb{R}$, $Q_\Gamma : \Gamma_Q \mapsto \mathbb{R}$, $M_\Gamma : \Gamma_M \mapsto \mathbb{R}$, find $w : \Omega \mapsto \mathbb{R}$ such that

$$D\Delta^2 w = g \qquad \text{in} \quad \Omega \tag{17}$$

$$w = w_\Gamma \qquad \text{on} \quad \Gamma_w \tag{18}$$

$$-\nabla w \cdot \boldsymbol{n} = \varphi_\Gamma \qquad \text{on} \quad \Gamma_\varphi \tag{19}$$

$$D\nabla(\Delta w) \cdot \boldsymbol{n} = Q_\Gamma \qquad \text{on} \quad \Gamma_Q \tag{20}$$

$$\nu D\Delta w + (1-\nu) D\boldsymbol{n} \cdot (\nabla\nabla w)\boldsymbol{n} = M_\Gamma \qquad \text{on} \quad \Gamma_M \tag{21}$$

Here, Δ denotes the Laplacian operator, g is a load per unit surface in the z direction, and $D = Et^3/[12(1-\nu^2)]$, where ν is the Poisson ratio, and t is the thickness of the plate. The rest of the notation is analogous to that of the one-dimensional case.

3.2. Numerical formulation

Here we present our discrete algorithm for Kirchhoff plates. Our discretization makes use of the finite-dimensional spaces generated by two-dimensional Non-Uniform Rational B-Splines (NURBS), which, in turn, originate from two-dimensional B-Splines.

3.2.1. Two-dimensional B-Splines

Let us define polynomial degrees p and q, and two open knot vectors $\boldsymbol{\Xi}$ and $\boldsymbol{\Upsilon}$. The parametric directions associated to them are denoted by ξ and η. The knot vector $\boldsymbol{\Xi}$ is defined by Eq. (6), while $\boldsymbol{\Upsilon} = (\eta_1, \eta_2, \ldots, \eta_{m+q+1})$. We note that the knot vectors $\boldsymbol{\Xi}$ and $\boldsymbol{\Upsilon}$ lead to bases $\{N_{i,p}(\xi)\}$ and $\{M_{j,q}(\eta)\}$ of dimensions n and m, respectively. Two-dimensional B-Splines can be defined by taking tensor products of their one-dimensional counterparts. Thus,

$$B_{ij,pq}(\xi,\eta) = N_{i,p}(\xi) M_{j,q}(\eta); \quad i = 1,\ldots,n, \quad j = 1,\ldots,m. \tag{22}$$

Let us call $\square$ the parameter space, that is, $\square = [\xi_1, \xi_{n+p+1}] \times [\eta_1, \eta_{m+q+1}]$. Let $\boldsymbol{\xi}$ be a generic point of $\square$. Using the functions (22), we can generate a geometrical object in the physical space $V_B = \boldsymbol{F}_B(\boldsymbol{\xi})$ by way of

the geometrical map $\boldsymbol{F}_B : \square \mapsto \Omega$ defined as

$$\boldsymbol{F}_B(\boldsymbol{\xi}) = \sum_{i=1}^{n}\sum_{j=1}^{m} \boldsymbol{C}_{ij} B_{ij}(\boldsymbol{\xi}) \quad \forall \xi \in \square \tag{23}$$

Here, $\boldsymbol{C}_{ij} \in \mathbb{R}^2$ are the control points of the object. Note also that in (23), and in what follows, we remove the reference to the polynomial orders in the sub-index of the functions B_{ij} for notational simplicity.

3.2.2. Non-Uniform Rational B-Splines (NURBS)

NURBS geometrical objects in $\mathbb{R}^2$ are projective transformations of B-Spline geometrical entities in $\mathbb{R}^3$. Let $\widehat{\boldsymbol{C}}_{ij} \in \mathbb{R}^2$ be a set of control points in two-dimensional space and W_{ij} a set of positive real numbers called *weights* such that $(\widehat{\boldsymbol{C}}_{ij}, W_{ij}) \in \mathbb{R}^3$. We define the following B-Spline geometrical object in $\mathbb{R}^3$ as,

$$\widehat{V} = \widehat{\boldsymbol{F}}(\square) \tag{24}$$

where

$$\widehat{\boldsymbol{F}}(\boldsymbol{\xi}) = \sum_{i=1}^{n}\sum_{j=1}^{m} (\widehat{\boldsymbol{C}}_{ij}, W_{ij}) B_{ij}(\boldsymbol{\xi}), \quad \boldsymbol{\xi} \in \square \tag{25}$$

The associated NURBS object V is defined as

$$V = \boldsymbol{F}(\square) \tag{26}$$

where the geometrical mapping $\boldsymbol{F}$ is defined as,

$$\boldsymbol{F}(\boldsymbol{\xi}) = \sum_{i=1}^{n}\sum_{j=1}^{m} \frac{\widehat{\boldsymbol{C}}_{ij}}{W_{ij}} \frac{W_{ij} B_{ij}(\boldsymbol{\xi})}{\sum_{k=1}^{n}\sum_{l=1}^{m} W_{kl} B_{kl}(\boldsymbol{\xi})}, \quad \boldsymbol{\xi} \in \square \tag{27}$$

Denoting,

$$\overline{\boldsymbol{C}}_{ij} = \frac{\widehat{\boldsymbol{C}}_{ij}}{W_{ij}}, \quad W(\boldsymbol{\xi}) = \sum_{i=1}^{n}\sum_{j=1}^{m} W_{ij} B_{ij}(\boldsymbol{\xi}) \tag{28}$$

and introducing the NURBS basis functions in parametric space

$$R_{ij}(\boldsymbol{\xi}) = \frac{W_{ij} B_{ij}(\boldsymbol{\xi})}{W(\xi)};\ i = 1, \ldots, n,\ j = 1, \ldots, m \tag{29}$$

we can rewrite the NURBS geometrical mapping as

$$\boldsymbol{F}(\boldsymbol{\xi}) = \sum_{i=1}^{n}\sum_{j=1}^{m} \overline{\boldsymbol{C}}_{ij} R_{ij}(\boldsymbol{\xi}), \quad \boldsymbol{\xi} \in \square. \tag{30}$$

3.2.3. Discrete space

NURBS basis functions in physical space are defined as the push forward of the functions R_{ij}, $i = 1, \ldots, n$, $j = 1, \ldots, m$. The discrete space that we will use for our numerical method is the space spanned by those functions, namely

$$\mathcal{V}^h = \text{span}\{R_{ij} \circ \boldsymbol{F}^{-1},\ i = 1, \ldots, n,\ j = 1, \ldots, m\}. \tag{31}$$

3.2.4. Collocation strategy: illustration of the algorithm with simplified boundary conditions

Our collocation strategy is sufficiently general to accommodate any combination of boundary conditions represented by Eqs. (18)–(21), but for the sake of a clear exposition, we start by describing our algorithm in a simplified case, where the same set of boundary conditions is applied on the entire boundary. Without loss of generality, we select the case of a simply supported plate, that is, $\Gamma_w = \Gamma_M = \Gamma$. The parametric space and the reference basis functions are defined by the knot vectors $\boldsymbol{\Xi}$ and $\boldsymbol{\Upsilon}$ (see Section 3.2.1), where we assume $p \geq 4$ and $q \geq 4$. Associated to this parametric space, we define nm Greville points as,

$$\hat{\boldsymbol{\tau}}_{ij} = \left(\frac{1}{p} \sum_{k=1}^{p} \xi_{i+k}, \frac{1}{q} \sum_{k=1}^{q} \eta_{j+k} \right); \; i = 1, \ldots, n; \; j = 1, \ldots, m \tag{32}$$

We note that those Greville points corresponding to $i = 1$, $i = n$, $j = 1$, and $j = m$ lie on the boundary of the parametric space, leading to a total of $2(n+m-2)$ boundary points. Making use of the geometrical map $\boldsymbol{F}$, the Greville points $\hat{\boldsymbol{\tau}}_{ij}$ may be pushed forward to the physical space as

$$\boldsymbol{\tau}_{ij} = \boldsymbol{F}(\hat{\boldsymbol{\tau}}_{ij}), \text{ for all } i = 1, \ldots, n; \; j = 1, \ldots, m. \tag{33}$$

As in the one-dimensional case, displacement boundary conditions are strongly enforced in the discrete space. Thus, let us define the space $\mathcal{V}_d^h = \{w^h \in \mathcal{V}^h | w^h = w_\Gamma^h \text{ on } \Gamma\}$, where w_Γ^h is an approximation to w_Γ living in the NURBS discrete space. A function of $\mathcal{V}_d^h$ can be constructed by taking a function of $\mathcal{V}^h$ and constraining the boundary control variables so as to achieve $w^h = w_\Gamma^h$ on Γ. Thus, $\dim(\mathcal{V}_d^h) = nm - 2(n + m - 2)$. Therefore, at this point we have $nm - 2(n + m - 2)$ unknowns that will be determined by collocating the partial-differential equation and the remaining boundary conditions at suitable Greville points. In particular, the partial-differential equation is collocated at the Greville points $\hat{\boldsymbol{\tau}}_{ij}$, skipping the two outermost layers, that is,

$$D\Delta^2 w^h(\hat{\boldsymbol{\tau}}_{ij}) = g(\hat{\boldsymbol{\tau}}_{ij}), \text{ for all } i = 3, \ldots, n-2; \; j = 3, \ldots, n-2 \tag{34}$$

which gives a total of $(n-4)(m-4)$ equations. Note that that number of remaining equations at this point is $\dim(\mathcal{V}_d^h) - (n-4)(m-4) = 2n + 2m - 12$ and we will use them to collocate the bending moment boundary condition at suitable Greville points. Note that we have exactly $2n + 2m - 4$ Greville points lying on the boundary so we do not have enough degrees of freedom to collocate Eq. (21) on all Greville boundary points, and a criterion to decide the collocation points that will be utilized needs to be defined. We adopt the following criterion: the corner points are skipped and the equations corresponding to the two closest points to the corner are averaged [see Figure 2(a)]. In this way, we use exactly $2n + 2m - 12$ equations to collocate the bending moment boundary condition, and we have a square linear system of equations. This completely defines our algorithm for simply supported plates.

Remark:

We acknowledge that we have no theoretical evidence for the accuracy of our method in multiple spatial dimensions at this point. However, we notice two important points: First, our choice to skip the corner collocation points is very convenient when solving certain types of mapped geometries. When the geometry is mapped, these points usually become singular, and it is not possible to define the derivatives of the

discrete solution at them. Thus, by skipping the corner points, the imposition of all types of boundary conditions becomes straightforward on arbitrary single-patch geometries, something that was not possible with our previously-proposed isogeometric collocation method for the Cahn-Hilliard equation [28]. Second, our numerical results (see Section 4) show excellent accuracy (in particular, patch tests are passed exactly – i.e., up to machine precision – for all the considered combinations of boundary conditions), stability, and robustness of the algorithm.

3.2.5. Collocation strategy in general situations

In this case, we only assume that Γ_w, Γ_φ, Γ_Q, and Γ_M are either the empty set or mappings of one (or several) of the boundary edges of the parametric domain. We notice that this restriction can also be removed, but we prefer to adopt the hypothesis for the sake of a clearer presentation. Again, we use a particular example to illustrate the algorithm, but the idea is trivially extended to any combination of boundary conditions. Here we focus on a plate that is simply supported on three of the boundary edges and fully clamped on the other one. Which one of the boundary edges is clamped is unimportant for the derivation of the algorithm, but to make the exposition precise, we assume that $\Gamma_\varphi = \boldsymbol{F}(\{\xi_1\} \times [\eta_1, \eta_{m+q+1}])$ where $\boldsymbol{F}$ is the geometrical mapping defined in Eq. (30). In addition, $\Gamma_w = \Gamma$. The remaining parts of the boundary, that is, Γ_Q and Γ_M are automatically defined by the conditions $\Gamma = \overline{\Gamma_w \cup \Gamma_Q} = \overline{\Gamma_\varphi \cup \Gamma_M}$, $\Gamma_w \cap \Gamma_Q = \emptyset$ and $\Gamma_\varphi \cap \Gamma_M = \emptyset$. In this case, the algorithm is analogous to that defined in Section 3.2.4 (simply supported plate), except in the way we average the equations corresponding to the collocated boundary conditions. Since averaging according to the strategy described in Section 3.2.4 would lead to averaging of equations that represent different boundary conditions in the corners where Γ_φ and Γ_M meet, we prefer to average over points on the same edge, as indicated in Figure 2(b).

Remark:

Extensive numerical testing in a number of different situations seems to indicate that averaging according to the strategy described in Section 3.2.4 (i.e., potentially averaging equations that represent different boundary conditions) does not influence at all accuracy. However, we preferred to present the modified strategy described in Section 3.2.5 for the sake of consistency.

4. Numerical examples

In this section we present and comment several numerical examples, which aim at showing the performance of the proposed formulation. The experiments have been selected in an attempt of testing the proposed method in different significant situations typical of engineering applications, keeping at the same time the presentation as concise as possible. Accordingly, the following three families of tests have been considered:

i. Beam patch tests (aiming at proving the accuracy of the boundary condition imposition strategy presented above);

ii. Square plate with a manufactured solution (aiming at showing that the same orders of convergence obtained for one-dimensional beams are attained also in the case of plates);

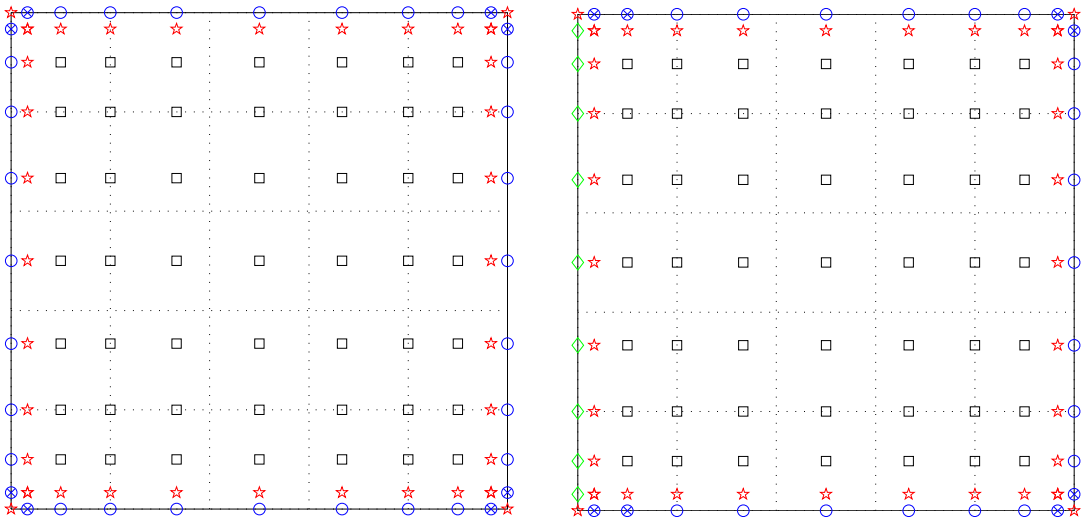

(a) Simply supported

(b) Clamped and simply supported

Figure 2: (Color online) Example of collocation points for the partial differential equation and collocated boundary conditions. We consider the parametric domain, we set degree $p = q = 6$ and the knot vectors $\boldsymbol{\Xi} = \boldsymbol{\Upsilon} = (0,0,0,0,0,0,0,.2,.4,.6,.8,1,1,1,1,1,1,1)$ in each direction, which leads to $n = m = 11$. All the marked points correspond to the nm Greville points as defined in Eq. (32). The points represented by (black) squares are used to impose the partial differential equation as illustrated in Eq. (34). The points represented by (red) stars are disregarded. For the simply supported plate (a), all the points represented with (blue) circles are used to collocate the bending moment boundary condition. Close to each corner point, the two equations associated to the (blue) circles with crosses are averaged to reduce the total number of equations by four. For the plate clamped on the left boundary and simply supported elsewhere (b), all the points represented with (blue) circles are used to collocate the bending moment boundary condition. Close to each corner point, the two equations associated to the (blue) circles with crosses are averaged to reduce the total number of equations by four. The points represented by (green) diamonds are used to collocate the rotation boundary condition.

iii. Simply supported circular plate (aiming at showing the good behavior of the proposed formulation and of the boundary condition imposition strategy also in the case of mapped geometries, possibly including singular points).

4.1. Beam patch tests

The aim of this section is to consider some examples such that the analytical solution may be exactly represented by the adopted approximation space. In such a way, several different boundary condition combinations may be tested allowing to evaluate the accuracy of the strategy proposed in the previous section.

To this end, we consider as a convenient patch test the problem of a Bernoulli-Euler beam with a uniformly distributed load and several combinations of end constraints (e.g., doubly clamped, simply supported, clamped-free or cantilever beam, etc.). Such problems may be studied by means of a Kirchhoff plate model with free-edge boundary conditions along the longitudinal sides and assuming $\nu = 0$. In all these cases, the analytical solution is constant transversally, while it consists of a quartic polynomial, satisfying the considered end conditions, longitudinally. Therefore, if the boundary condition imposition strategy is accurate, even one quartic knot span should be able to represent the analytical solution exactly (i.e., up to machine precision).

In fact, all performed numerical tests, considering several combinations of boundary conditions, different meshes (of one or more knot spans), and different degrees (greater or equal to four), confirm that these kinds of patch tests are passed up to machine precision (data not shown), guaranteeing the quality of the proposed strategy.

4.2. Square plate with a manufactured solution

We now study a clamped plate, defined over the bi-unit square $[0, 1]^2$, with a sinusoidal load constructed starting from a manufactured solution. Assuming material properties such that $D = 1$, the considered analytical solution and the corresponding distributed load are, respectively:

$$w(x, y) = [1 - \cos(2\pi x)][1 - \cos(2\pi y)] \tag{35}$$

$$g(x, y) = -16\pi^4[\cos(2\pi x) - 4\cos(2\pi x)\cos(2\pi y) + \cos(2\pi y)] \tag{36}$$

Convergence plots of the L^2-norm error for w, φ_x, Q_x, and M_x are reported in Figure 3 for degrees $p = q = 4, \dots, 9$. It is possible to observe that the same orders of convergence obtained in the beam case (i.e., $p - 2$ or $p - 3$ for even or odd degree p, respectively) are attained, and that for all quantities a very similar convergence behavior is in general obtained. Convergence plots of the other components of rotation, shear force, and bending moment are completely analogous and are not reported here for the sake of brevity.

Finally, a similar test has been carried out also in the case of a simply supported plate, and analogous results have been obtained.

4.3. Simply supported circular plate

As a last example, we consider a simply supported plate, defined over a circular domain of radius $R = 1$, with a uniformly distributed load, assumed here to be $g(x, y) = 1$. Material properties are assumed such that

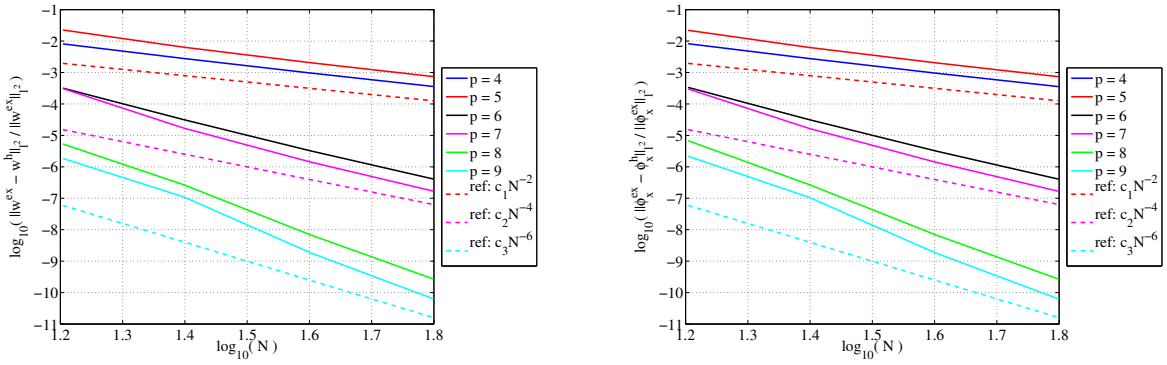

(a) Deflection

(b) Rotation

(c) Shear force

(d) Bending moment

Figure 3: (Color online) Square plate with a manufactured solution. Convergence plots of the L^2-norm error for w (a), φ_x (b), Q_x (c), and M_x (d) as a function of the number of control points per parametric direction N and for different degrees $p = q$.

$D = 1$. For this problem, an analytical expression for the deflection at the center of the plate is classically known to be:

$$w_0 = \frac{5+\nu}{64(1+\nu)} \tag{37}$$

Convergence plots of the deflection of the center of the plate, normalized with respect to the exact solution, are reported in Figure 4 for different approximation degrees $p = q = 4, \dots, 7$ (the Poisson ratio is assumed to be $\nu = 0.3$). As shown in Figure 4, the proposed isogeometric collocation method provides a good approximation of the solution also in the case of mapped geometries, even with relatively coarse meshes.

We highlight that the map transforming the parameter space in the physical space is in this case such that each edge of the parameter space corresponds to a quarter of circle, and the four corners of the parameter space correspond to four singular points on the boundary (see the details of the mapping, for example, in [42]). The adopted strategy for boundary condition imposition is able to efficiently deal with situations like this, as confirmed by these (and several further) numerical experiments.

Finally, a similar test has been carried out also in the case of a clamped plate, and analogous results have been obtained.

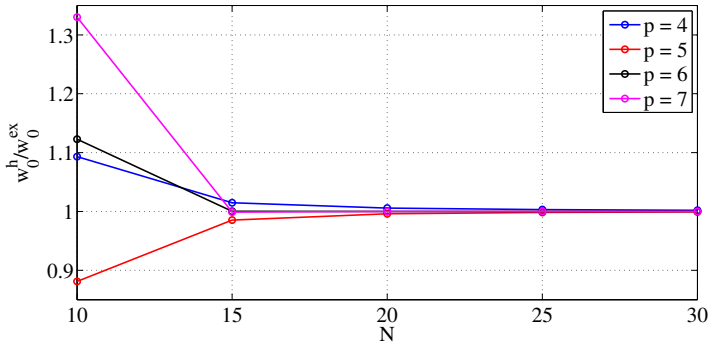

Figure 4: (Color online) Simply supported circular plate. Convergence plot of the displacement at the center of the plate as a function of the number of control points per parametric direction N and for different degrees $p = q$.

5. Conclusions

This paper presents a new isogeometric collocation method for thin structural elements governed by Bernoulli-Euler beam and Kirchhoff plate models. Our algorithm is geometrically flexible, achieves the expected convergence rates for all quantities of engineering interest, and permits straightforward imposition of boundary conditions on arbitrary single-patch mapped geometries, even in the presence of singular points. Our numerical results show the accuracy, stability, and robustness of the method. We believe that the notable approximation capabilities of the method, as well as its computational efficiency, will place it in the body of literature as a viable and flexible option for the solution of thin structural problems.

6. Acknowledgements

HG was partially supported by the European Research Council through the FP7 Ideas Starting Grant (project no. 307201). HG was also partially supported by Xunta de Galicia, and by Ministerio de Economía y Competitividad (contract # DPI2013-44406-R). The last two grants are cofinanced with FEDER funds. AR was partially supported by the European Research Council through the FP7 Ideas Starting Grant (project no. 259229) *ISOBIO - Isogeometric Methods for Biomechanics* and by the Italian MIUR through the FIRB "Futuro in Ricerca" Grant RBFR08CZ0S *Discretizzazioni Isogeometriche per la Meccanica del Continuo*. This support is gratefully acknowledged.

The authors would finally like to thank G. Sangalli (University of Pavia) and T.J.R. Hughes (University of Texas at Austin) for several fruitful discussions on the presented formulations.

References

[1] I. Akkerman, Y. Bazilevs, V. M. Calo, T. J. R. Hughes, S. Hulshoff, The role of continuity in residual-based variational multiscale modeling of turbulence, *Computational Mechanics* **41** 371–378, 2007.

[2] F. Auricchio, L. Beirao da Veiga, A. Buffa, C. Lovadina, A. Reali, G. Sangalli, A Fully Locking-free Isogeometric Approach for Plane Linear Elasticity Problems: a Stream Function Formulation, *Computer Methods in Applied Mechanics and Engineering*, **197** 160–172, 2007.

[3] F. Auricchio, L. Beirao da Veiga, T.J.R. Hughes, A. Reali, G. Sangalli, Isogeometric Collocation Methods, *Mathematical Models and Methods in Applied Sciences*, **20** 2075–2107, 2010.

[4] F. Auricchio, L. Beirao da Veiga, T.J.R. Hughes, A. Reali, G. Sangalli, Isogeometric collocation for elastostatics and explicit dynamics, *Computer Methods in Applied Mechanics and Engineering*, **249-252** 1043–1055, 2012.

[5] F. Auricchio, L. Beirao da Veiga, C. Lovadina, A. Reali, The importance of the exact satisfaction of the incompressibility constraint in nonlinear elasticity: mixed FEMs versus NURBS-based approximations. *Computer Methods in Applied Mechanics and Engineering*, **199** 314–323, 2010.

[6] F. Auricchio, L. Beirao da Veiga, J. Kiendl, C. Lovadina, A. Reali, Locking-free isogeometric collocation methods for spatial Timoshenko rods, submitted to *Computer Methods in Applied Mechanics and Engineering*, 2012.

[7] F. Auricchio, F. Calabrò, T.J.R. Hughes, A. Reali, G. Sangalli. Efficient Quadrature for NURBS-based Isogeometric Analysis. *Computer Methods in Applied Mechanics and Engineering*, **249-252** 15–27, 2012.

[8] Y. Bazilevs, V.M. Calo, J.A. Cottrell, T.J.R. Hughes, A. Reali, G. Scovazzi, Variational multiscale residual-based turbulence modeling for large eddy simulation of incompressible flows, *Computer Methods in Applied Mechanics and Engineering* **197** 173–201, 2007.

[9] Y. Bazilevs, T.J.R. Hughes, NURBS-based isogeometric analysis for the computation of flows about rotating components, *Computational Mechanics* **43** 143–150, 2008.

[10] L. Beirao da Veiga, C. Lovadina, A. Reali, Avoiding shear locking for the Timoshenko beam problem via isogeometric collocation methods, *Computer Methods in Applied Mechanics and Engineering* **249-252** 2–14, 2012.

[11] M.J. Borden, C.V. Verhoosel, M.A. Scott, T.J.R. Hughes, C.M. Landis, A phase-field description of dynamic brittle fracture, *Computer Methods in Applied Mechanics and Engineering* **217** 77–95, 2012.

[12] A. Buffa, C. de Falco, G. Sangalli, IsoGeometric Analysis: Stable elements for the 2D Stokes equation, *International Journal for Numerical Methods in Fluids* **65**, 1407–1422, 2011.

[13] J.F. Caseiro, R.A.F. Valente, A. Reali, J. Kiendl, F. Auricchio, R.J. Alves de Sousa, On the Assumed Natural Strain method to alleviate locking in solid-shell NURBS-based finite elements. *Computational Mechanics* doi:10.1007/s00466-014-0978-4, 2014.

[14] J.A. Cottrell, T.J.R. Hughes, Y. Bazilevs, Isogeometric Analysis: Toward integration of CAD and FEA, Wiley, 2009.

[15] J.A. Cottrell, T.J.R. Hughes, A. Reali, Studies of refinement and continuity in isogeometric structural analysis, *Computer Methods in Applied Mechanics and Engineering*, **196** 4160–4183, 2007.

[16] J.A. Cottrell, A. Reali, Y. Bazilevs, T.J.R. Hughes, Isogeometric Analysis of Structural Vibrations, *Computer Methods in Applied Mechanics and Engineering*, **195** 5257–5296, 2006.

[17] R.P. Dhote, H. Gomez, R N.V. Melnik, J. Zu, Isogeometric analysis of a dynamic thermo-mechanical phase-field model applied to shape memory alloys, *Computational Mechanics*, **53**(6), 1235–1250, 2014.

[18] C. de Falco, A. Reali, R. Vázquez. GeoPDEs: a research tool for IsoGeometric Analysis of PDEs, *Advances in Engineering Software*, **42** 1020–1034, 2011.

[19] J. Liu, H. Gomez, J.A. Evans, T.J.R. Hughes, C.M. Landis, Functional entropy variables: A new methodology for deriving thermodynamically consistent algorithms for complex fluids, with particular reference to the isothermal NavierStokesKorteweg equations, *Journal of Computational Physics*, **248**, 47–86, 2014.

[20] L. De Lorenzis, J.A. Evans, A. Reali, T.J.R. Hughes, Isogeometric Collocation: Neu- mann boundary conditions and contact. *ICES Report* 14-06, 2014.

[21] T. Elguedj, Y. Bazilevs, V.M. Calo, T.J.R. Hughes, $\bar{B}$ and $\bar{F}$ projection methods for nearly incompressible linear and non-linear elasticity and plasticity using higher-order NURBS elements, *Computer Methods in Applied Mechanics and Engineering* **197** 2732–2762, 2008.

[22] H. Gomez, V.M. Calo, Y. Bazilevs, T.J.R. Hughes, Isogeometric analysis of the Cahn-Hilliard phase-field model, *Computer Methods in Applied Mechanics and Engineering* **197** 4333–4352, 2008.

[23] H. Gomez, T.J.R. Hughes, X. Nogueira, V.M. Calo, Isogeometric analysis of the isothermal Navier-Stokes-Korteweg equations, *Computer Methods in Applied Mechanics and Engineering* **199** 1828–1840, 2010.

[24] H. Gomez, T.J.R. Hughes, Provably unconditionally stable, second-order time-accurate, mixed variational methods for phase-field models, *Journal of Computational Physics*, **230**, 5310–5327, 2011.

[25] H. Gomez, X. Nogueira, An unconditionally energy-stable method for the phase-field crystal equation, *Computer Methods in Applied Mechanics and Engineering* **249–252**, 52–61, 2012.

[26] H. Gomez, X. Nogueira, A new space-time discretization for the Swift-Hohenberg equation that strictly respects the Lyapunov functional, *Communications in Nonlinear Science and Numerical Simulation* **17**(12), 4930–4946, 2012.

[27] H. Gomez, J. París, Numerical simulation of asymptotic states of the damped Kuramoto-Sivashinsky equation, *Physical Review E*, **83**, 046703, 2011.

[28] H. Gomez, A. Reali, G. Sangalli, Accurate, efficient, and (iso)geometrically flexible collocation methods for phase-field models, *Journal of Computational Physics*, **262**, 153–171, 2014.

[29] T.J.R. Hughes, J.A. Cottrell, Y. Bazilevs, Isogeometric analysis: CAD, finite elements, NURBS, exact geometry and mesh refinement, *Computer Methods in Applied Mechanics and Engineering*, **194** 4135–4195, 2005.

[30] T.J.R. Hughes, J.A. Evans, A. Reali, Finite Element and NURBS Approximations of Eigen- value, Boundary-value, and Initial-value Problems. *Computer Methods in Applied Mechanics and Engineering*, **272** 290–320, 2014.

[31] T.J.R Hughes, A. Reali, G. Sangalli, Duality and unified analysis of discrete approximations in structural dynamics and wave propagation: comparison of p-method finite elements with k-method NURBS, *Computer Methods in Applied Mechanics and Engineering*, **197** 4104–4124, 2008.

[32] T.J.R. Hughes, A. Reali, G. Sangalli, Efficient Quadrature for NURBS- based Isogeometric Analysis. *Computer Methods in Applied Mechanics and Engineering*, **199** 301–313, 2010.

[33] J. Kiendl, F. Auricchio, L. Beirao da Veiga, C. Lovadina, A. Reali, Isogeometric collocation methods for the Reissner-Mindlin plate problem. Submitted, 2014.

[34] J. Kiendl, F. Auricchio, T.J.R. Hughes, A. Reali, Single-variable formulations and isogeometric discretizations for shear deformable beams. Submitted, 2014.

[35] J. Kiendl, Y. Bazilevs, M.-C. Hsu, R. Wüchner, K.-U. Bletzinger. The bending strip method for isogeometric analysis of Kirchhoff–Love shell structures comprised of multiple patches. *Computer Methods in Applied Mechanics and Engineering*, **199** 2403–2416, 2010.

[36] J. Kiendl, K.-U. Bletzinger, J. Linhard, R. Wüchner, Isogeometric Shell Analysis with Kirchhoff-Love Elements, *Computer Methods in Applied Mechanics and Engineering*, **198** 3902–3914, 2009.

[37] S. Morganti, F. Auricchio, D.J. Benson, F.I. Gambarin, S. Hartmann, T.J.R. Hughes, A. Reali, Patient-specific isogeometric structural analysis of aortic valve closure. *ICES Report* 14-10, 2014.

[38] S. Lipton, J.A. Evans, Y. Bazilevs, T. Elguedj, T.J.R. Hughes, Robustness of isogeometric structural discretizations under severe mesh distortion, *Computer Methods in Applied Mechanics and Engineering*, **199** 357–373, 2010.

[39] A. Reali, An Isogeometric Analysis Approach for the Study of Structural Vibrations, *Journal of Earthquake Engineering*, **10**, 1–30, 2006.

[40] D. Schillinger, J.A. Evans, A. Reali, M.A. Scott, T.J.R. Hughes, Isogeometric Collocation: Cost Comparison with Galerkin Methods and Extension to Adaptive Hierarchical NURBS Discretizations, *Computer Methods in Applied Mechanics and Engineering*, **267** 170–232, 2013.

[41] D. Schillinger, S.J. Hossain, T.J.R. Hughes, Reduced Bezier element quadrature rules for quadratic and cubic splines in isogeometric analysis, *Computer Methods in Applied Mechanics and Engineering*, **277** 1–45, 2014.

[42] A.-V. Vuong, Ch. Heinrich, B. Simeon, ISOGAT: A 2D tutorial MATLAB code for Isogeometric Analysis, *Computer Aided Geometric Design*, **27**(8), 644–655, 2010.